Quasi-two-dimensional perturbations in duct flows under transverse magnetic field

A. Pothérat[a)]
Ilmenau Technical University, Kirchhoffstrasse 1, 98693 Ilmenau, Germany

(Received 9 February 2007; accepted 8 May 2007; published online 27 July 2007)

Inspired by the experiment from Moresco and Alboussiere [J. Fluid Mech. **504**, 167 (2004)], we study the stability of a flow of liquid metal in a rectangular, electrically insulating duct with a steady homogeneous magnetic field perpendicular to two of the walls. In this configuration, the Lorentz force tends to eliminate the velocity variations in the direction of the magnetic field. This leads to a quasi-two-dimensional base flow with Hartmann boundary layers near the walls perpendicular to the magnetic field, and so-called Shercliff layers in the vicinity of the walls parallel to the field. Also, the Lorentz force tends to strongly oppose the growth of perturbations with a dependence along the magnetic field direction. On these grounds, we represent the flow using the model from Sommeria and Moreau [J. Fluid Mech. **118**, 507 (1982)], which essentially consists of two-dimensional (2D) motion equations with a linear friction term accounting for the effect of the Hartmann layers. The simplicity of this quasi-2D model makes it possible to study the stability and transient growth of quasi-two-dimensional perturbations over an extensive range of nondimensional parameters and reach the limit of high magnetic fields. In this asymptotic case, the Reynolds number based on the Shercliff layer thickness $\mathrm{Re}/H^{1/2}$ becomes the only relevant parameter. Tollmien-Schlichting waves are the most linearly unstable mode as for the Poiseuille flow, but for $H \gtrsim 42$, a second unstable mode, symmetric about the duct axis, appears with a lower growth rate. We find that these layers are linearly unstable for $\mathrm{Re}/H^{1/2} \gtrsim 48350$ and energetically stable for $\mathrm{Re}/H^{1/2} \lesssim 65.32$. Between these two bounds, some nonmodal quasi-two-dimensional perturbations undergo some significant transient growth (between two and seven times more than in the case of a purely 2D Poiseuille flow, and for much more subcritical values of Re). In the limit of a high magnetic field, the maximum gain $G_{\max}$ associated with this transient growth is found to vary as $G_{\max} \sim (\mathrm{Re}/\mathrm{Re}_c)^{2/3}$ and occur at time $t_{G_{\max}} \sim (\mathrm{Re}/\mathrm{Re}_c)^{1/3}$ for streamwise wavenumbers of the same order of magnitude as the critical wavenumber for the linear stability. © *2007 American Institute of Physics*. [DOI: 10.1063/1.2747233]

I. INTRODUCTION

Liquid metal flows in rectangular ducts under imposed magnetic fields are important for the metallurgy as well as for the design of the future ITER nuclear fusion reactor. The simplest case of a uniform magnetic field parallel to the side wall of the duct has received considerable attention from theoreticians and experimentalists over the past 50 years. References 3 and 4 clearly identified the three main regions of the flow in the laminar regime for the case of insulating walls perpendicular to the magnetic field. The problem is governed by the Reynolds number Re and the Hartmann number Ha, the square of which represents the ratio between the Lorentz and the viscous forces, as well as by the aspect ratio of the duct. For large values of Ha (typically more than 10), Hartmann boundary layers with a simple exponential profile and a thickness of Ha^{-1} develop along these walls. These were first discovered by Hartmann (Ref. 5) and further demonstrated by Shercliff (Ref. 6). Far from the walls, the Lorentz force strongly damps the velocity variations along the magnetic field lines so that the flow is two-dimensional, as explained by Sommeria and Moreau (Ref. 2) and Davidson (Ref. 7). The boundary layers which arise along the side walls, now called Shercliff layers, have a complex three-dimensional profile of thickness $a/\mathrm{Ha}^{-1/2}$ (a is the duct dimension along the field) found analytically by Shercliff (Ref. 3).

The next step was to investigate the stability of the flow. Probably because of its simpler base profile, the Hartmann layer has received the most attention: linear stability analyses performed by several authors agree to a critical Reynolds number around $\mathrm{Re}/\mathrm{Ha} \simeq 48000$,[8–10] whereas the energy stability analysis provides a sufficient condition for stability for $\mathrm{Re}/\mathrm{Ha} < 25$.[10–12] More recently, it has been suggested that some nonmodal perturbations may undergo significant transient growth,[13,14] and direct numerical simulation (DNS) performed by Krasnov *et al.* (Ref. 15) showed that the nonlinear evolution of such perturbations leads to a destabilization of the Hartmann layer for $\mathrm{Re}/\mathrm{Ha} > 390$. All of these works, however, involve either a channel flow geometry or a flow over an infinite plate, none of which include any Shercliff layers. This has the advantage of clarifying the properties of the Hartmann layer itself but raises difficult questions when it comes to comparison with experiments in which the presence of side walls, and therefore Shercliff layers, cannot be

[a)]Electronic mail: alban.potherat@tu-ilmenau.de

avoided. Many such experimental data have been produced on duct flows in the past half-century.[16–18] In particular, the most recent experiment from Ref. 1 was conducted with the sole purpose of finding the instability threshold for the Hartmann layer. It consists of measuring the total friction in a toroidal square duct placed inside a 13*T* superconducting magnet. In the limit of large values of Ha, they find the instability threshold to be Re/Ha=380. The excellent agreement between this result and the channel flow DNS of Krasnov *et al.*[15] suggests that the stability of the Hartmann layer is hardly or not affected by the presence of the side walls. It, however, leaves open the question of whether the Shercliff layers and the core flow are laminar or turbulent when the Hartmann layers destabilize. The value of the friction measured in Ref. 1 when the Hartmann layer is laminar recovers quite closely the friction given by the laminar Hartmann layer theory: this indicates at least that no 3D turbulence exists in this regime as this would produce a strong extra Joule and viscous dissipation. The possibility, however, that the flow is in a quasi-2D turbulent state producing only a small extra dissipation cannot be written off. This is supported by recent studies performed in Ilmenau on the transient growth of perturbations in a channel flow between two parallel walls with a magnetic field parallel to these walls. It was found that for Ha$\gtrsim$100, vortices aligned with the magnetic field are the perturbations undergoing maximum transient growth, as opposed to the classical Poiseuille case (without magnetic field) where streamwise-independent perturbations are the most amplified (not published yet).

In view of these considerations, the aim of the present work is to undertake a first step toward tackling the question of the stability of Shercliff layers by studying their stability against quasi-two-dimensional perturbations. By quasi-two-dimensional, we mean that the velocity field is assumed independent of the coordinate along the magnetic field lines (this is usually referred to as the 2D core assumption), except in the vicinity of the Hartmann walls (those orthogonal to the magnetic field), where it exhibits the classical exponential profile of Hartmann layers. To this end, we use the model from Ref. 2 (thereafter SM82), which assumes quasi-two-dimensionality as well as the fact that the Hartmann layers remain laminar. It provides a two-dimensional equation for the flow motion in the average plane orthogonal to the magnetic field where the effect of the Hartmann layers is taken into account through a linear friction term. Comparisons between theory and experiments have shown that this model renders the two-dimensional dynamics of the parallel layers to a very good approximation (in particular, friction and turbulent properties[19,20] as well as some stability properties[21,22]). Reference 19 has furthermore demonstrated that the 2D model departs from the 3D solution of Ref. 4 by less than 10%. On this basis, we use the SM82 model to study the sensitivity of Shercliff layers to quasi-two-dimensional perturbations. This means all flow patterns derived from this model exhibit a Hartmann flow profile in the direction of the magnetic field and a velocity field to be determined in the plane orthogonal to that direction. The layout of this work is as follows. In Sec. II, we briefly recall the model from Ref. 2 and the associated quasi-2D base solution for the duct flow. The important question of the relevance of the SM82 model to the full 3D profile of the Shercliff layers is also reviewed. We then study the linear stability of this solution in Sec. III, which provides a sufficient condition for instability. A necessary condition for instability is obtained from the energy stability analysis in Sec. IV. Section V is then devoted to the search of nonmodal perturbations undergoing maximal transient growth. We finally come back to the experiment of Ref. 1 in conclusion and briefly discuss it in the light of this work.

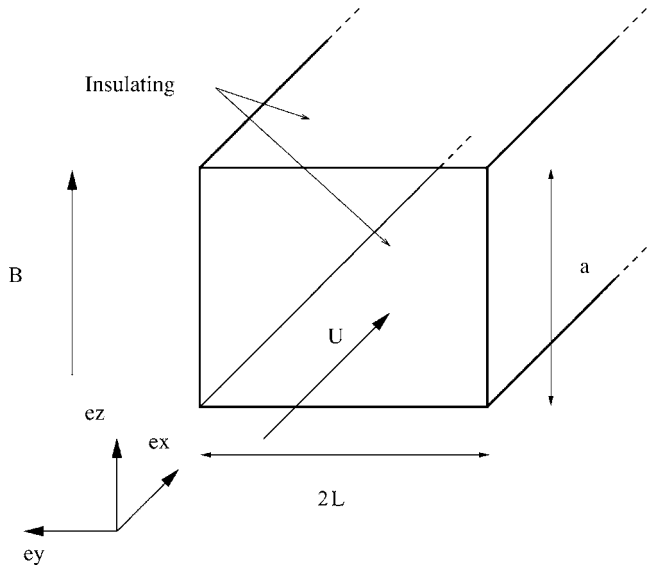

FIG. 1. Problem geometry: the top and bottom (Hartmann) walls are electrically insulating (wall conductivity $\sigma_W=0$) and the electric current normal to the side walls is imposed.

II. BASIC EQUATIONS: 2D MODEL FOR THE DUCT FLOW

We consider an electrically conducting fluid (electric conductivity σ, kinematic viscosity ν, density ρ) flowing through a duct of rectangular cross section (height a, width $2L$) and subjected to a steady homogeneous magnetic field perpendicular to the top and bottom walls of the duct (as sketched in Fig. 1).

For a strong enough magnetic field, this flow is known to be quasi-two-dimensional, that is, the velocity hardly varies along the direction of the magnetic field, except in Hartmann boundary layers, which develop along the top and bottom plates. Assuming these layers remain laminar, the flow is well described by averaging the quasistatic magnetohydrodynamics (MHD) equations along the magnetic field direction. This results in the Sommeria and Moreau model (SM82) governing the evolution of the average velocity, given here in nondimensional form,[2,19]

$$\nabla \cdot \mathbf{u} = 0,$$
$$\partial_t \mathbf{u} + \mathbf{u} \cdot \nabla \mathbf{u} + \nabla p = \frac{1}{\mathrm{Re}}(\nabla^2 \mathbf{u} - H\mathbf{u} + \mathbf{f}). \tag{1}$$

Re is the Reynolds number $\mathrm{Re}=U_0 L/\nu$ based on the maximum velocity of the base profile U_0. The parameter H

$=n(L^2/a^2)aB\sqrt{\sigma/(\rho\nu)}$ is a measure of the friction term [with characteristic dimensional Hartmann friction time $t_H=na/B\sqrt{\rho/(\sigma\nu)}$], which represents the effect of the Lorentz force on the flow. n represents the number of Hartmann layers in the problem: here $n=2$, but the case of a rigid upper free surface could be handled by setting $n=1$. The flow is driven by a constant force density $\mathbf{f}$ (nondimensional), which can result either from a pressure gradient G imposed along the duct (i.e., dimensionally, $\mathbf{f}_{\mathrm{dim}}=G\mathbf{e}_x$) or from a transverse electric current density J_0 imposed at the side walls (i.e., dimensionally, $\mathbf{f}_{\mathrm{dim}}=J_0B\mathbf{e}_x$, as in the experiment from Ref. 1). The model (1) can thus describe all cases with imposed electric current at the side walls, as well as the case of insulating walls for which $J_0=0$. The case of a pressure-driven flow where the side walls have a finite conductivity studied experimentally by Ref. 23 requires a slightly different model such as that from Ref. 21. The simple form of this equation is interesting as it places the problem studied here within the more general framework of the 2D flows with an arbitrary linear friction. On these grounds, we shall not restrict ourselves to the high values of H and H^2/Re, which correspond to a dominant Lorentz force, and for which (1) is indeed a good approximation of the 3D MHD flow.

Using the no-slip boundary conditions at the side walls,

$$\mathbf{u}(y=-1)=\mathbf{u}(y=1)=0, \tag{2}$$

the base flow is found as an exact solution of (1) and (2) of the form $\mathbf{U}=U(y)\mathbf{e}_x$ with

$$\frac{H}{f}U(y)=1-\frac{\cosh\sqrt{H}y}{\cosh\sqrt{H}}. \tag{3}$$

Since velocities are normalized by the maximum velocity of the base profile U_0, the latter is related to the driving force by

$$U_0=\frac{L^2}{\rho\nu}\frac{f_{\mathrm{dim}}}{H}\left(1-\frac{1}{\cosh\sqrt{H}}\right) \tag{4}$$

and (3) can be rewritten as

$$U(y)=\frac{\cosh\sqrt{H}}{\cosh\sqrt{H}-1}\left(1-\frac{\cosh\sqrt{H}y}{\cosh\sqrt{H}}\right). \tag{5}$$

In the limit $H\to 0$, (5) recovers the two-dimensional Poiseuille profile whereas for high values of H, the profile is almost flat, except in the vicinity of the walls located at $y=1$ and -1, where it exhibits boundary layers of thickness $H^{-1/2}$. The full 3D solution also features some boundary layers of the same thickness at this location, which are now commonly called Shercliff layers. Their physical mechanism can be understood as follows: Ref. 2 has shown that the Lorentz force acts so as to diffuse the momentum of a structure of size $l_\perp$ along the magnetic field lines over a length $l_\parallel$ within a characteristic time,

$$\tau_{2\mathrm{D}}=\frac{\rho}{\sigma B^2}\frac{l_\parallel^2}{l_\perp^2}. \tag{6}$$

This diffusion results from current loops between plans orthogonal to the magnetic field. If $\tau_{2\mathrm{D}}$ is shorter than all other time scales, in particular those of inertia $\tau_u=l_\perp/U$ and of viscous friction $\tau_\nu^\parallel=l_\parallel^2/\nu$ and $\tau_\nu^\perp=l_\perp^2/\nu$, then the momentum just outside the Hartmann layer is instantaneously diffused to the whole core flow and the flow is quasi-two-dimensional. The thickness of the parallel layers (including Shercliff layers) is precisely the scale at which $\tau_{2\mathrm{D}}\sim\tau_\nu^\perp$, as they are determined by the balance between the Lorentz force and the viscous friction in planes orthogonal to the field. This means that in those layers, viscous friction has had time to act on the flow before the momentum outside the Hartmann layers has had time to diffuse to the rest of the parallel layer. Since the diffusion is not complete, the profile of parallel layers is not 2D, and the Shercliff layers result from the balance between viscous friction and part of the momentum present outside the Hartmann layer.

In the SM82 model, parallel layers result from a balance between the term representing the friction of the Hartmann layer on the flow and viscous friction in planes orthogonal to the field: it is therefore a simplification of the dynamics of the Shercliff layers that assumes that the momentum just outside the Hartmann layer still diffuses instantly to the whole parallel layer. This results in 2D layers, in which viscous friction balances the whole of the momentum outside the Hartmann layer. In order to evaluate the loss due to this simplification, Ref. 19 has compared these 2D and 3D profiles (see Fig. 2 from Ref. 19) and has shown that the 3D profile does not depart from (5) by more than about 10%. This indicates that in spite of the action of viscosity, the quasi-two-dimensionality assumption is only slightly violated in the Shercliff layers. Since the physics of the 2D model and that of the 3D Shercliff layers are therefore close—but not quite identical—the SM82 model is expected to provide some relevant indications on the 2D dynamics of the 3D Shercliff layers, even though it obviously misses the 3D dynamics. This has been found to be the case in many instances in which theoretical results derived from the 2D model have been compared to experiments: Refs. 20 and 24 have performed DNSs of (1) and a refined version of it, and found that both the friction and fine turbulent properties of the parallel layer are recovered in great detail. Perhaps more importantly for the present study, the critical Reynolds number and wavelength for the instability of a free parallel layer (which exhibits the same kind of three-dimensionality as the Shercliff layers) measured by Ref. 22 are in excellent agreement with the prediction of Ref. 21 based on a variant of (1) taking Hartmann wall conductivity into account.

On this basis, it is reasonable to expect (1) to provide a relevant description of the dynamics of quasi-2D perturbations in the Shercliff layers. This approach should, however, not be expected to give the last word on the stability of those layers. Instead, it should be considered as a toy-model that incorporates most, but not all, of the physics of the full 3D problem. Ultimately, the effect of three-dimensionality and 3D perturbations will have to be determined by full 3D DNS or a numerical resolution of the 3D stability problem. Either of these, however, involve some high computational costs, which preclude any parametric study or high values of H. Such analyses can be performed with the 2D model, and the obtained result can be used to guide future 3D computations performed for selected values of H and Re.

A further advantage of the SM82 approach is that it does not reflect the physics of the MHD problem only, but also that of any 2D flow with linear friction of any origin. The results derived in the forthcoming sections are therefore exact mathematical properties of this class of models.

III. LINEAR STABILITY ANALYSIS

A. Mathematical formulation

We shall start the stability analysis by studying the stability of (5) to infinitesimal perturbations. This provides a sufficient condition for instability. To this end, the perturbed velocity profile (and according pressure) is decomposed as

$$\mathbf{u} = \mathbf{U} + \hat{\mathbf{u}}(y)\exp[i(kx - \omega t)], \tag{7}$$

where it has been taken advantage of the invariance in the x direction to write the perturbation as a normal mode. The evolution equation for $v(y) = \hat{\mathbf{u}}(y) \cdot \mathbf{e}_y$ is obtained by linearization of (1) around the solution (5). After elimination of the pressure, this reduces to the following eigenvalue problem:

$$\mathcal{L}_{OS} v = -i\omega \mathcal{M} v,$$

$$-\mathcal{L}_{OS} = ikU\mathcal{M} + ikU'' + \frac{1}{\mathrm{Re}}\mathcal{M}^2 + \frac{H}{\mathrm{Re}}\mathcal{M}, \tag{8}$$

$$\mathcal{M} = k^2 - D^2$$

with boundary conditions $v(-1) = v(1) = 0$. D is the differentiation operator with respect to y, and the U' denotes the y derivative of U. The Orr-Sommerfeld operator $\mathcal{L}_{OS}$ only differs from the usual Orr-Sommerfeld operator, which appears in the linear stability analysis of hydrodynamic parallel flows through the additional friction term, so both problems can be made formally identical by introducing the frictionless eigenvalue $\omega_0 = \omega - H/i\mathrm{Re}$, as noticed by Thess (Ref. 25).

B. Numerical procedure

The eigenvalue problem (8) is solved numerically using MATLAB. To this end, we use a spectral discretization based on Tchebychev polynomials in the y direction, making sure that there are a least 10 collocation points in each of the intervals $[-1, -1+H^{-1/2}]$ and $[1-H^{-1/2}, 1]$, and at least 100 within $[-1, 1]$. Our numerical resolution follows that presented in detail in Ref. 26, and the MATLAB routines we use to solve the eigenvalue problem are essentially adapted from the routines given there. For each chosen value of $H \in [0, 10^4]$, we look for the lowest value of Re such that the maximum eigenvalue $\omega_m(k_m)$ has a positive imaginary part, corresponding to the first unstable mode (the corresponding quantities are thereafter referred to as *critical*). This is done using a simple dichotomy method, with a relative precision of 10^{-5} on both the critical Reynolds number Re_c and the critical wavenumber, which achieves the maximum growth rate k_c. We tested our algorithm on the 2D Poiseuille problem ($H=0$) and recovered the known values of $\mathrm{Re}_c(H=0) = 5772,22$ and $k_c(H=0) = 1.02$ found for instance in Ref. 26. We also calculated the critical Reynolds and wavenumber with twice as many collocation points as mentioned above for $H=1$, 10, 100, and 1000. The difference was below the specified relative precision of 10^{-5}. The same method has been used to determine the critical curve in the (Re, k) plane (i.e., the smallest and highest values of the unstable wavenumbers at given Re).

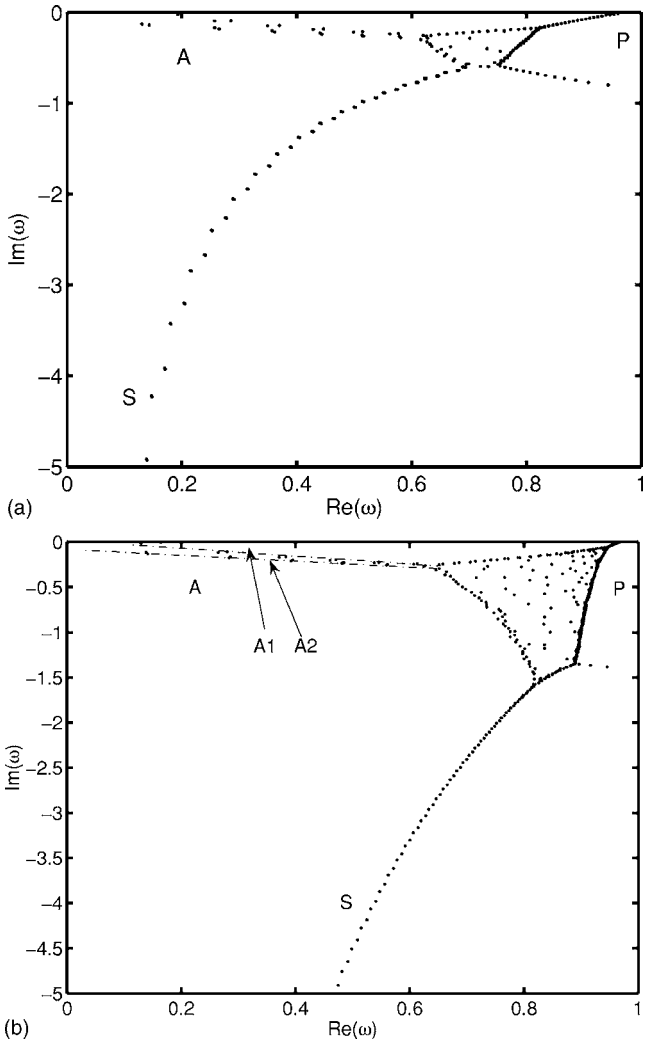

FIG. 2. Spectra of ω near criticality for $H=10$ (top) and $H=100$ (bottom). For $H=10$, $\mathrm{Re}_c = 4.40223 \times 10^5$ and $k_c = 1.73896$.

C. Results

Figure 2 shows the eigenvalue spectra of ω from the discretized operator $-i\mathcal{M}^{-1}\mathcal{L}_{OS}$ near criticality, for several values of H. The spectra exhibit the same three branches as those labeled A, P, and S in Ref. 27 for the case of the plane Poiseuille flow ($H=0$). As H increases, the number of weakly dissipated modes along the P branch increases faster than that along the A branch. These modes correspond to vortex patterns developing in the center of the channel (see Fig. 3). However, the first unstable mode to appear is always one of the A branch. This critical mode is mostly the quasi-2D MHD equivalent of the Tollmien-Schlichting waves in Poiseuille flows. Additionally, a center region of growing size and filling density when H increases appears at the junction of the A, P, and S branches. A similar behavior has already been observed in Ref. 13 in the case of the 3D

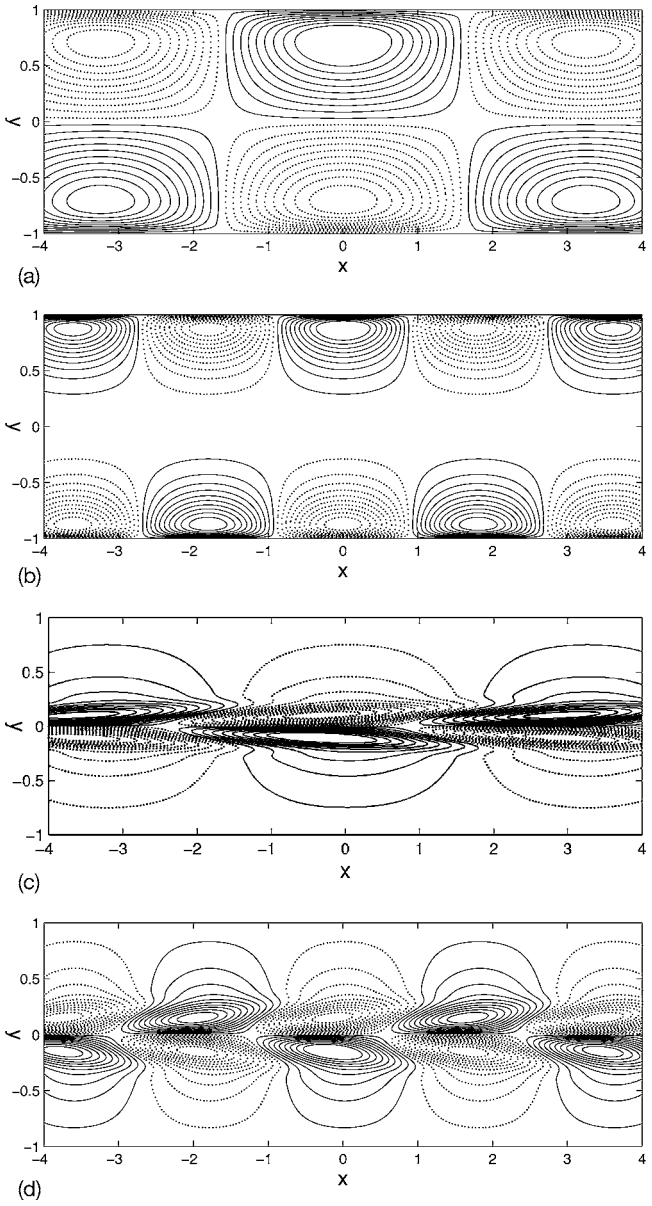

FIG. 3. Real part of the normalized streamfunction of the eigenmodes of the $-i\mathcal{M}^{-1}\mathcal{L}_{OS}$ operator for $H=10$ (left) and $H=100$ (right). Critical mode from the A branch (see Fig. 2) (top) and least dissipative mode from the P branch (bottom). The dotted lines correspond to negative values of the streamfunction while solid lines represent positive values.

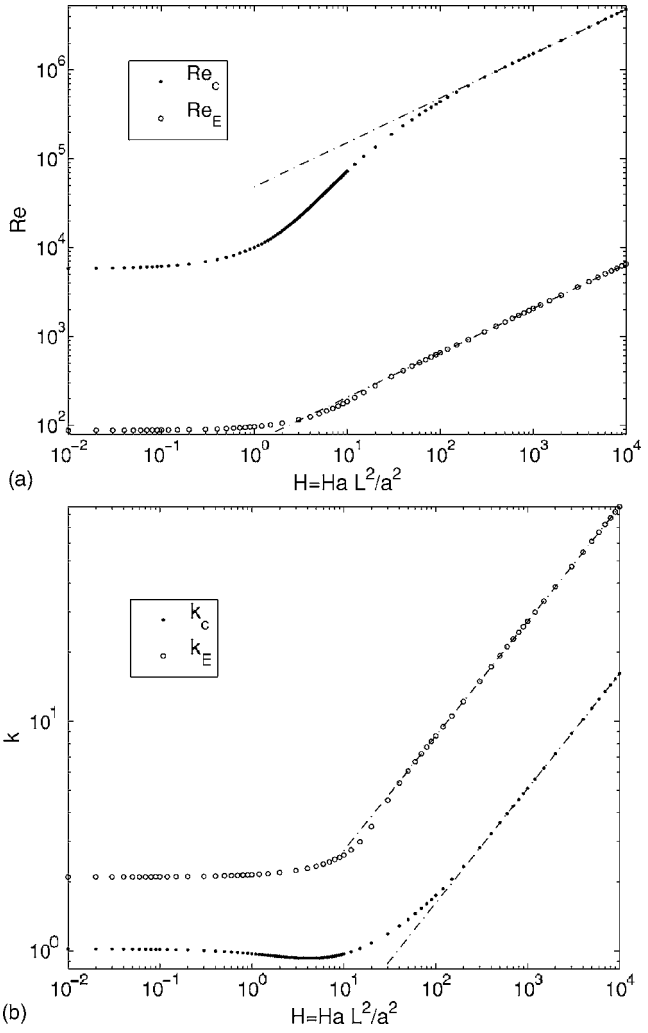

FIG. 4. Critical Reynolds number (top) and critical wavenumber (bottom) obtained from the linear stability analysis (Sec. III) and the energy stability analysis (Sec. IV). These two critical Reynolds numbers provide, respectively, an upper and a lower bound for the stability threshold. The points correspond to the effectively calculated values.

Hartmann channel flow problem. Reference 28 has shown that the appearance of this region at the branch junctions in the Orr-Sommerfeld problem associated with the Poiseuille flow was due to finite numerical precision. Since (8) is formally identical to the Orr-Sommerfeld equation for the Poiseuille flow, as only the base profiles differ, this result also applies here. The affected eigenvalues, however, have a large negative imaginary part so they do not affect the stability results presented here. Therefore, and in order to keep computational costs low, the numerical precision was not increased beyond 64 bits.

The critical Reynolds and wavenumbers are plotted in Fig. 4, together with their critical counterpart obtained from the energy stability analysis (see Sec. IV). In the limit $H \to 0$, we recover the critical values for the 2D Poiseuille flow, as mentioned in Sec. III B. An asymptotic regime appears in the limit $H \to \infty$ (in practice for H higher than around 200), for which $\mathrm{Re}_c = 4.83504 \times 10^4 H^{1/2}$ and $k_c = 0.161532 H^{1/2}$. In this case, the boundary layers at $y=-1$ and $y=1$ do not interact with each other, so the problem is governed by the stability property of each boundary layer. The length scale L becomes irrelevant and the problem is governed solely by the Reynolds number based on the thickness of the Shercliff layer $\mathrm{Re}/H^{1/2}$. Interestingly, the critical wavenumber $k_c(H)$ reaches a minimum of $k_c^{\min} = 0.92736 \pm 8 \times 10^{-5}$ for $H = 4.2 \pm 0.1$, i.e., between these two asymptotic regimes.

High values of the critical Reynolds number scaled on the boundary layer thickness close to that found here also characterize the stability of suction layers[29] and Hartmann layers.[8,10] The reason for this similarity is that even though the governing equations for these three problems differ [for example, the governing equations for the Hartmann layer

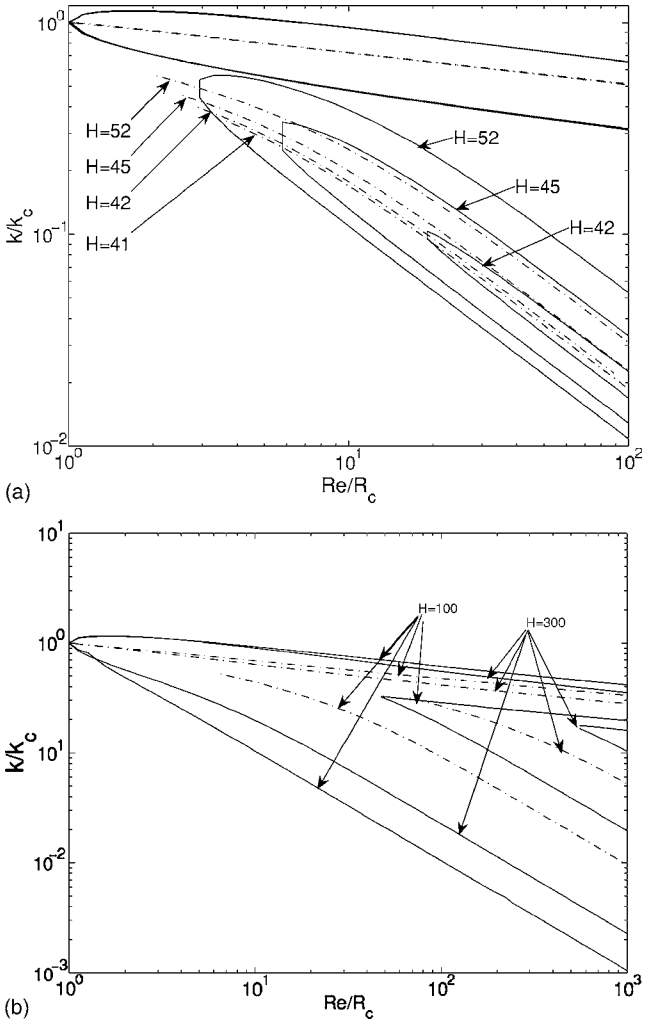

FIG. 5. Neutral stability curves (solid lines) and wavenumber of maximal growth rate (dash-dot) as a function of the parameter $\mathrm{Re}/\mathrm{Re}_c$ for several values of H. For low values of H around 45, the two branches of instabilities are separated. The upper branch hardly varies between $H=41$ and 52, whereas the lower one changes significantly (top). The maximum of the growth rate due to the eigenvalue of the A2 branch exists also for values of Re where it is not positive (also for $H<42$). For higher values of H, the two branches merge (bottom). For $H\sim 300$, the upper branch has reached an asymptotic curve in the plane $(\mathrm{Re}/\mathrm{Re}_c, k/k_c)$, whereas the lower one has not.

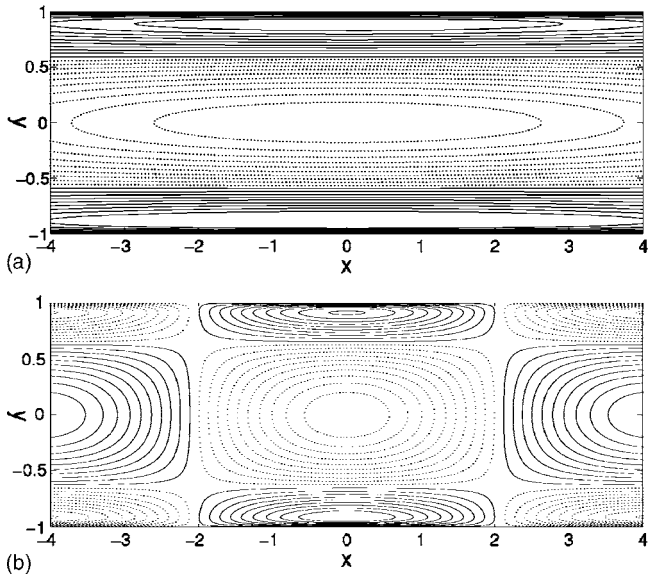

FIG. 6. Most unstable mode of the lower branch for $H=100$, $\mathrm{Re}/\mathrm{Re}_c=100$ (left, the corresponding wavelength is $k=0.09222k_c$, and the two branches are separated for this value of Re) and for $H=300$, $\mathrm{Re}/\mathrm{Re}_c=96.17$ (right, the corresponding wavelength is $k=0.02711k_c$, and the two branches are not separated for this value of Re, see Fig. 5).

have an extra term involving the electric potential not present in (1)], all three boundary layers have an exponential base profile.

A deeper insight into the linear stability of the flow can be gained with help of the neutral curves, which represent the border between stable and unstable modes in the $(\mathrm{Re}/\mathrm{Re}_c, k/k_c)$ plane. These are plotted in Fig. 5, along with the curves for the wavelength achieving maximal growth rate. The first noticeable feature is that the unstable modes are located in relatively narrow bandwidths which drift toward the lower wavenumbers as Re increases. This rather contrasts with the large high-pitched bandwidth over which transient growth occurs, as will be seen in Sec. V. The second noticeable feature is that the set of unstable modes is split into two branches. The upper (lower) branch stems from the most unstable mode of the A1 (A2) subbranch of the eigenvalue spectrum (see Fig. 2). The modes from the upper branch are the Tollmien-Schlichting waves mentioned earlier in this section, the most unstable of which is always more unstable than that of the lower one. The modes corresponding to the lower branch are made of one strong vortex in each of the boundary layers and one weaker central one. In contrast to the antisymmetric critical modes of the upper branch (see Fig. 3), they are symmetric about the center of the duct (Fig. 6). At low values of H, the lower branch is separated from the upper one and appears at increasing values of Re and k^{-1} when H decreases. We could not find this lower branch for $H<42$, but it is difficult to tell from our discrete numerical calculation whether it is there as it could persist at much higher values of Re and k^{-1}. When H increases, the lower branch merges into the upper and keeps moving toward very high Re, whereas the upper branch converges toward an asymptotic curve in the plane $(\mathrm{Re}/\mathrm{Re}_c, k/k_c)$.

IV. ENERGY STABILITY ANALYSIS

A. Principle and formulation

We now seek a lower bound for the Reynolds number at which the base flow (5) becomes unstable. Such a lower bound is obtained by looking for the maximum value of the Reynolds number Re_E for which the energy $E=\|\tilde{\mathbf{u}}\|^2$ of any given perturbation $\tilde{\mathbf{u}}=\mathbf{u}-\mathbf{U}$ decays monotonically (here the functional norm is the usual $\mathcal{L}_2$ norm). Following Ref. 30, we start from the equation governing the evolution of E, which is readily derived from (1),

$$\frac{1}{2}\frac{dE}{dt}=-i\omega_E[\tilde{\mathbf{u}}]E, \tag{9}$$

$$-i\omega_E[\tilde{\mathbf{u}}] = -\frac{\int \tilde{\mathbf{u}}\cdot\mathbf{D}[\mathbf{U}]\tilde{\mathbf{u}}d\Omega + (1/\mathrm{Re})\|\nabla\tilde{\mathbf{u}}\|^2}{E} - \frac{H}{\mathrm{Re}}. \quad (10)$$

D denotes the deformation tensor based on the laminar solution (5), $D_{ij}=1/2(\partial_{x_i}U_{x_j}+\partial_{x_j}U_{x_i})$. Let now S be the subspace of $\mathcal{L}_2$ spanned by solenoidal vector fields that satisfy the no-slip boundary conditions at the side walls. Then Re_E is the highest value of Re such that the maximum of the functional $i\omega_E[\tilde{\mathbf{u}}]$ over S is negative. This optimization problem is solved using variational calculus and introducing a Lagrange multiplier to enforce the constraint of mass conservation. After elimination of the latter, the maximum value of ω_E and the function that achieves it are found to be solutions of the following eigenvalue problem:

$$\mathcal{L}_E v = -2i\omega\mathcal{M}v,$$
$$\mathcal{L}_E = ik(U'' + 2\mathbf{U}'D) + \frac{2}{\mathrm{Re}}\mathcal{M}^2 - 2\frac{H}{\mathrm{Re}}\mathcal{M}. \quad (11)$$

Contrary to the eigenvectors of $i\mathcal{M}^{-1}\mathcal{L}_{OS}$, which are a solution of the linearized motion equations, and would therefore correspond to a possibly observable flow pattern if linear instability were the driving mechanism, those of $i/2\mathcal{M}^{-1}\mathcal{L}_E$ are no solutions of the motion equations. This partly explains that the lower bound given by the energy stability analysis often lays far below any observed instability threshold. It, however, has the advantage of not relying on any assumption made either on the equations or on the perturbations. In particular, finite amplitude perturbations are counted in. Here again, the introduction of the frictionless growth rate $\omega_{E0}=\omega_E-H/i\mathrm{Re}$ makes (11) formally identical to the hydrodynamic Poiseuille problem.

B. Results

Since the eigenvalue problems (8) and (11) only differ through the expression of the linear operators involved, (11) is solved using the same numerical method and procedure as for the linear stability analysis (see Sec. III B).

A distinctive feature of the 2D energy stability analysis, as opposed to the 3D one, is that there cannot be any solenoidal perturbation satisfying $k=0$. In the 3D channel flow problem without magnetic field, Refs. 30 and 31 have shown that these streamwise-independent perturbations are precisely those achieving the maximum energy growth rate. This remarkable property, therefore, cannot be extended to flows governed by a 2D equation.

The spectra of eigenvalues of $i/2\mathcal{M}^{-1}\mathcal{L}_E$ possess only one branch and the related eigenfunctions correspond to vortex-like patterns regularly spread across the channel width. The number of vortices increases as the eigenvalue tends to $-\infty$. The critical mode is always made of two rows of antisymmetric vortices, as shown on Fig. 7.

The dependence on H of the critical Reynolds Re_E and streamwise wavenumber k_E for the energy stability analysis are shown in Fig. 4. Contrary to the critical wavelength for the linear stability, that for the energy stability increases monotonically with H. In the limit $H\to\infty$, the energy stability threshold for the flow is that of a single side boundary layer, characterized by the single critical parameter $\mathrm{Re}_E/H^{1/2}=65.3288$. The related wavelength of the critical mode tends to $k_E=0.863484H^{1/2}$.

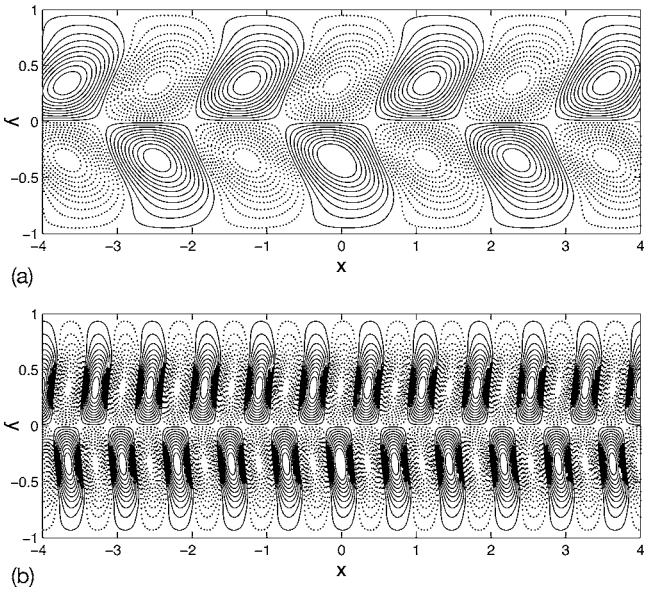

FIG. 7. Critical modes for the energy stability for $H=10$ (left, $\mathrm{Re}_E=1.84703\times10^2$, $k_E=2.61287$), $H=100$ (right, $\mathrm{Re}_E=6.53225\times10^2$, $k_E=8.62501$).

V. TRANSIENT GROWTH

A. Principle and formulation

In the two preceding sections, we found an upper and a lower bound for the threshold of the instability occurring in the channel. The lower bound has been obtained as a "no perturbation growth" condition, as all perturbations decay monotonically for $\mathrm{Re}<\mathrm{Re}_E$. The fact that it departs strongly from the upper bound, which corresponds to a condition for infinitesimal perturbations to grow, leaves open the possibility for some perturbations to still grow between these two extremes. Such a growth is known to stem from the nonnormality of the Orr-Sommerfeld operator. For such operators, a linear combination of eigenmodes of the operator can undergo a short but possibly intense transient growth, even though each normal mode decays monotonically. Reference 15 showed that in the Hartmann layer problem, such grown perturbations can act as finite-amplitude disturbances and destabilize the mean flow well below the linear stability threshold. Since this mechanism is likely to also play a key role in our problem, we shall now complete our overview of the quasi-2D stability of the MHD duct flow by estimating the maximum transient growth associated with the two-dimensional dynamics of Eq. (1).

The detailed method to find the maximal transient growth and the associated perturbations can be found, for instance, in Ref. 26. It consists of solving the nonmodal linearized perturbation equation,

$$\mathcal{L}_{OS}v = \mathcal{M}\partial_t v, \tag{12}$$

by expanding the perturbation over the set of Orr-Sommerfeld modes, with a vector of associated time-dependent coefficients $\kappa=(\kappa_1,\ldots,\kappa_N)$, with N large enough. The so-discretized solution v_N of (12) is then expressed as a function of the diagonal matrix built from the eigenvalues of the Orr-Sommerfeld operator $\mathbf{\Lambda}=\mathrm{diag}(\omega_1,\ldots,\omega_N)$:

$$\kappa(t) = \kappa(t=0)\exp(-it\mathbf{\Lambda}). \tag{13}$$

Defining the maximum gain reached at time t over the set of possible initial perturbations as $G(t)=\max(\|\kappa(t)\|)(\|\kappa(t=0)\|)$, then $G(t)$ is expressed as the square of the principal singular value $\sigma_1(t)$ of the matrix $C=F\exp(-it\Lambda)F^{-1}$, where $\mathcal{M}=F^HF$ is the Hermitian decomposition of $\mathcal{M}$. The left singular vector associated with $\sigma_1(t)$ represents the normalized initial perturbation achieving maximum growth at time t (thereafter called optimal perturbation at time $t=0$), and the right singular vector associated with $\sigma_1(t)$ represents the vector field into which this same perturbation evolves at time t (thereafter optimal perturbation at time t). It should also be underlined that $G(t)$ does not represent the time evolution of any one perturbation but rather the envelope of the family of curves representing the evolution of all perturbations becoming at some time the most amplified.

B. Numerical procedure

We solve the problem numerically using the same expansion in Tchebychev polynomials as for the linear and energy stability analysis (see Sec. III B). The singular value decomposition is performed with the standard MATLAB routine. This yields for given values of H, Re, and k the growth $G(t)$ of the optimal perturbation at time t.

These calculations are repeated for $H\in\{0,1,3,10,30,100,300,1000\}$. For each value of H, we take 10 values of Re in geometric progression between $\mathrm{Re}_E(H)$ and $\mathrm{Re}_c(H)$ and 10 in geometric progression between $\mathrm{Re}_c(H)$ and $100\mathrm{Re}_c(H)$ in order to reach clean asymptotics. k is taken in the interval $[0,6k_c]$. Since we are interested in the maximum transient growth over time, we start by calculating 10 values of $G(t)$ and then refine the calculation around the maximum until a relative precision of 10^{-3} over $G_{mk}=\max_t G(t)$, and 10^{-3} over t_G [defined by $G(t_G)=G_{mk}$] is reached. The G_{mk} maxima are gathered to provide a $G_{mk}(k)$ profile for each value of (H,Re) and the same procedure as above is used to determine the maximum growth over k, $G_{\max}$, and associated wavenumbers $k_{G_{\max}}$ and time $t_{G_{\max}}$.

Additionally, the number of modes used for the linear and energy stability (see Sec. III B) turned out to be insufficient to resolve the strong shear of the optimal modes in supercritical regime. The resolution had to be multiplied by 1.2 for $\mathrm{Re}>\mathrm{Re}_c$ and progressively increased up to a factor 2.5 for $\mathrm{Re}=100\mathrm{Re}_c$ in order to keep the variations of G_{mk} and $G_{\max}$ with the number of modes under the prescribed precision.

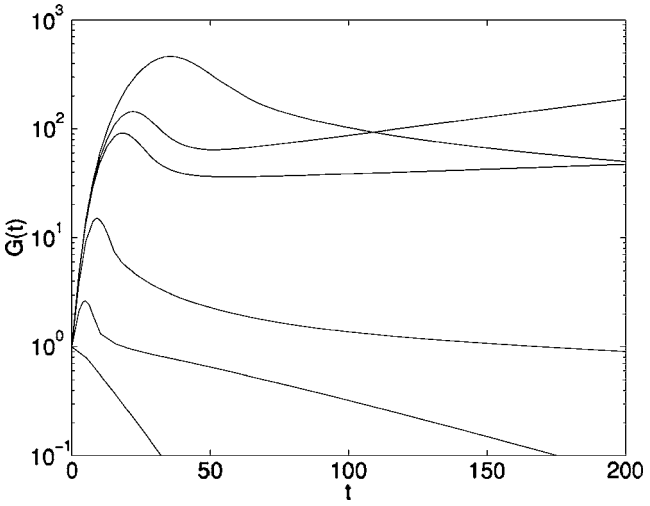

FIG. 8. $G(t)$ for $H=100$, $\mathrm{Re}<\mathrm{Re}$, $\mathrm{Re}/\mathrm{Re}_c=0.01$, 0.1, 1.1, 2, and 10 (by order of growing maximum). For $\mathrm{Re}<\mathrm{Re}_c$, no growth occurs. For $\mathrm{Re}/\mathrm{Re}_c=1.1$ and 2, the Tollmien-Schlichting wave of streamwise wavelength k_c grows exponentially. This, however, happens quite a long time after a combination of modes of streamwise wavenumber k_c undergo some significant transient growth. For $\mathrm{Re}/\mathrm{Re}_c=10$, the normal modes of wavelength k_c are no longer in the unstable bandwidth, but a combination of them still undergoes transient growth.

C. Optimal modes given *H*, *R*, *k*, and *t*

The evolution of $G(t)$ is found to be qualitatively similar to that known for the two-dimensional Poiseuille flow (see, for instance, Ref. 26, p. 115). For $\mathrm{Re}<\mathrm{Re}_E$, since the energy stability returns a no growth condition, $G(t)$ monotonically decays from $G(t=0)=1$ to 0 when $t\to\infty$, and this for all values of k. For $\mathrm{Re}_E<R<\mathrm{Re}_c$, there exist some values of k for which $G(t)$ first increases, reaches a maximum at $t=t_G$, and then decays to 0. For $\mathrm{Re}>\mathrm{Re}_c$, $G(t)$ still exhibits a local maximum but diverges when $t\to\infty$ for the wavelengths with linearly unstable normal modes. This means that there are modes undergoing transient growth as soon as $\mathrm{Re}>\mathrm{Re}_E$ and that even for $\mathrm{Re}>\mathrm{Re}_c$, transient growth exists and happens at a much earlier time than any substantial exponential growth from the linearly unstable modes identified in Sec. III. Some examples of these different cases are gathered in Fig. 8.

The optimal modes are plotted in Figs. 9 and 10. As in the case of the energetic and linear stability, the scale of the transversal velocity variations follows that of the Shercliff layer thickness, so that both at $t=0$ and at the time of maximal growth t_G, the optimal perturbation presents an increasing number of vortices along the spanwise direction as H increases. When the Reynolds number is increased, the streamlines of the optimal perturbation at $t=0$ undergo a stronger shear from the base flow so that for high enough values of Re, vortices degenerate in streaks of alternate vorticity that become more and more aligned with the streamwise direction as Re is further increased.

Remarkably, at $t=t_G$, the optimal perturbation always evolves into modes that resemble the critical normal modes found in Sec. III. The general aspect of these optimal perturbations is very similar to that of those found in the case of the infinite channel with spanwise magnetic field parallel to

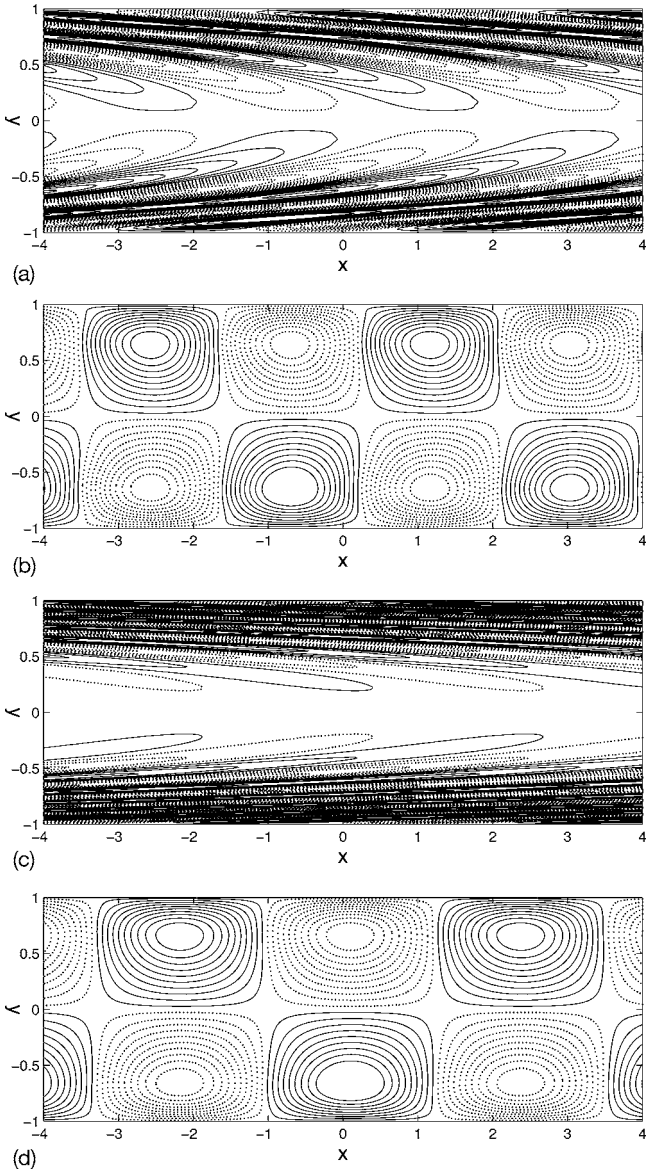

FIG. 9. Streamlines of the optimal perturbation achieving $G_{\max}$ for $H=10$, $\mathrm{Re}/\mathrm{Re}_c=0.1366$ (top), $\mathrm{Re}/\mathrm{Re}_c=2.783$ (bottom). In both cases, the mode with strong shear (left) represents the perturbation at $t=0$ and the flow on the right represents the same perturbation at $t=t_{G\max}$ (right).

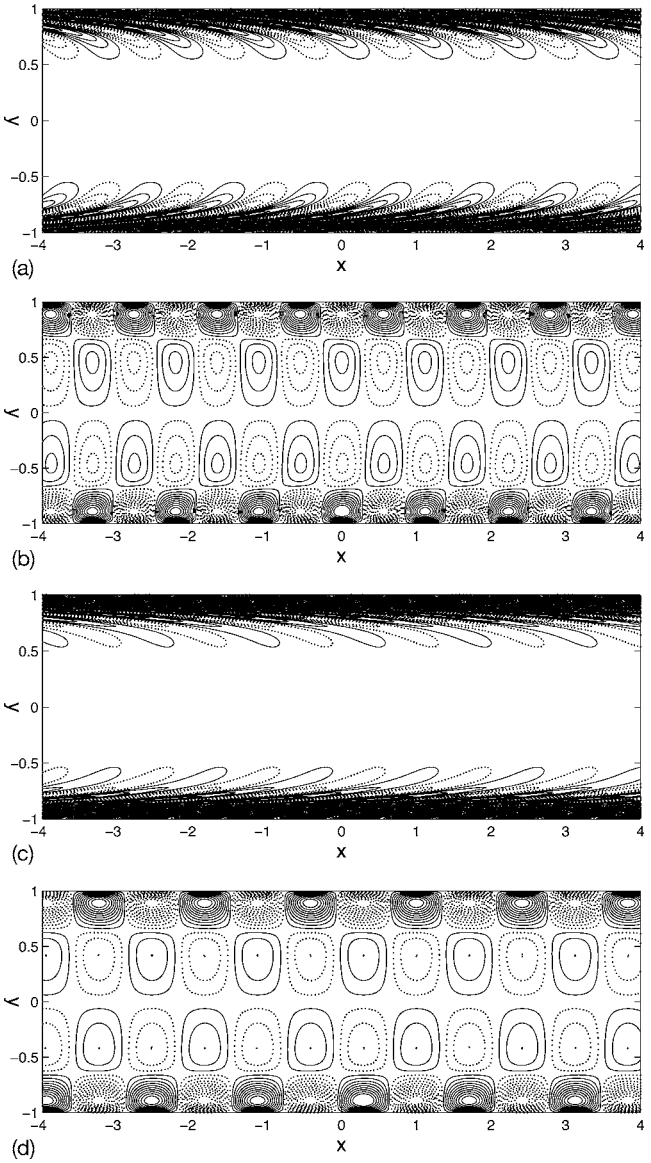

FIG. 10. Streamlines of the optimal perturbation, $H=100$, $\mathrm{Re}/\mathrm{Re}_c=0.1141$ (top) and $\mathrm{Re}/\mathrm{Re}_c=2.783$ (bottom). Optimal perturbation at $t=0$ (left) and $t=t_{G\max}$ (right).

the walls: by searching the optimal perturbations with possible dependence in the three spatial directions, it is found that for $\mathrm{Ha}\gtrsim 100$, the optimal perturbations are 2D and aligned with the magnetic field. For lower values of Ha, although these perturbations do undergo some transient growth, other perturbations with wave vector of nonzero component along **B** (therefore three-dimensional) achieve the maximum growth. The strong similarity between the two problems suggests that in the limit of large H, the quasi-2D optimal perturbations found in this section for the duct problem may well undergo a stronger transient growth than any other possible 3D perturbations not taken into account in the present work. Of course, this remains to be proved—or disproved—by a 3D analysis in the exact duct configuration.

D. Maximum transient growth over *k* and over time, for given *H* and Re

We shall now characterize more quantitatively how the optimal modes, their associated wavelength, growth rate, and time of maximum growth rate vary with H and Re. Figure 11 shows the variations of the local maximum G_{mk} of $G(t)$ as well as those of t_G as a function of k, for $H=100$ and Re varying from the critical $\mathrm{Re}_E(H=100)$ to $100\mathrm{Re}_c(H=100)$. When transient growth exists, $G_{mk}(k)$ reaches a maximum $G_{\max}$ for $k=k_m(\mathrm{Re},H)$. As opposed to the linear stability, which only yields narrow bandwidths of unstable wavenumbers, some significant transient growth occurs on a broad, high-pitched bandwidth extending much further than our maximum calculated value of $k/k_c=6$ for $H>100$.

Figure 12 shows the variations of $G_{\max}$ as a function of $\mathrm{Re}/\mathrm{Re}_c(H)$ for different values of H. All curves are rather close to each other, which means that the maximum gain is

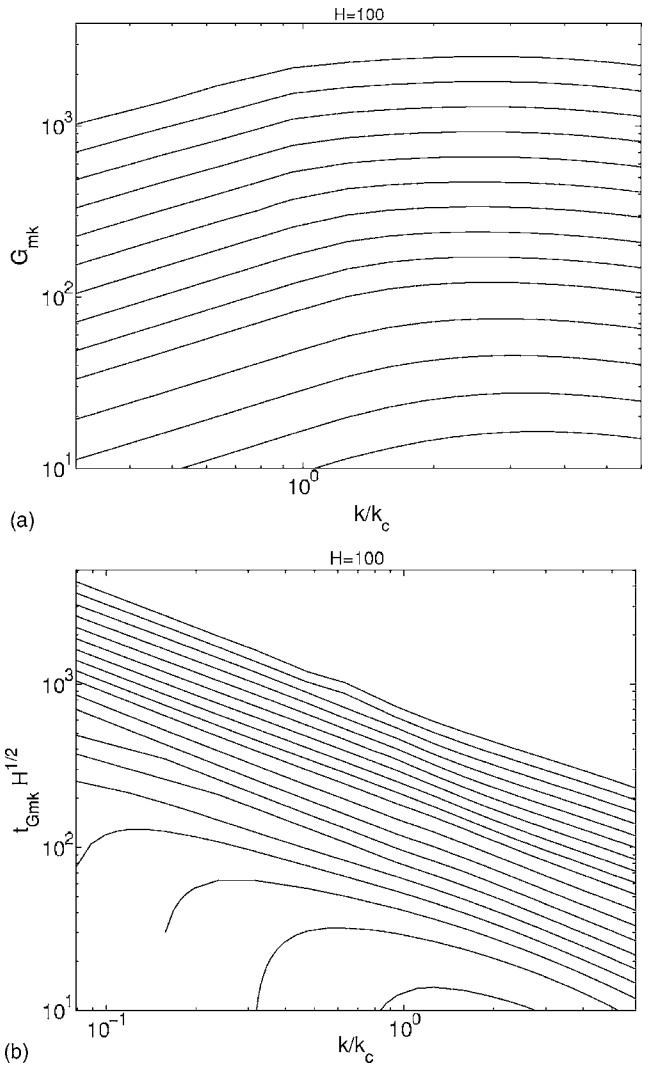

FIG. 11. Maximum transient growth (top) and time of maximum transient growth (bottom) as a function of the streamwise wavenumber k, for $H=100$, and for 10 values of Re in geometric progression between $\mathrm{Re}_E(H=100)$ and $\mathrm{Re}_c(H=100)$ and 10 between $\mathrm{Re}_c(H=100)$ and $100\mathrm{Re}_c(H=100)$.

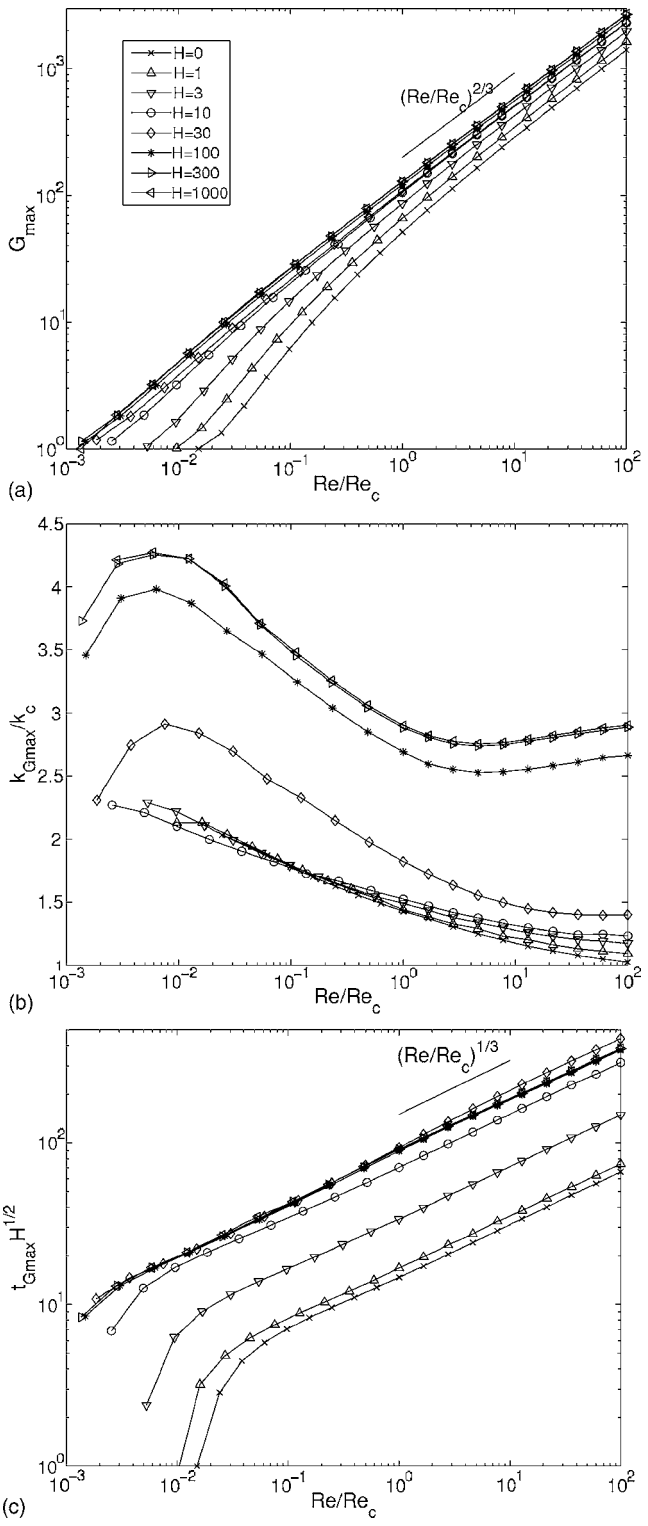

FIG. 12. Maximum transient growth $G_{\max}$ over time and streamwise wavenumber (top), streamwise wavenumber of maximum transient growth $k_{G\max}$ (middle) and time of maximum transient growth $t_{G\max}$ (bottom) as a function of $\mathrm{Re}/\mathrm{Re}_c$ for $H\in\{0,1,3,10,30,100,300,1000\}$. The curves for $H=300$ and 1000 cannot be distinguished, which proves once again that good asymptotics are reached for a value of H of a few hundred. For $H=0$, $t_{G\max}$ and not $t_{G\max}H^{1/2}$ vs $\mathrm{Re}/\mathrm{Re}_c$ is represented.

mostly controlled by the parameter $\mathrm{Re}/\mathrm{Re}_c(H)$. This becomes exact as H tends to infinity since all curves rapidly approach an asymptotic exponential law of the form $G_{\max}\sim(\mathrm{Re}/\mathrm{Re}_c)^{2/3}$. This exponent of Re is smaller than that of 2 obtained for the maximum transient growth in 3D Poiseuille flow, mostly because the optimal perturbations for the 3D Poiseuille flow are streamwise independent. Since such perturbation cannot exist in two-dimensional dynamics, the maximum transient growth is achieved by streamwise dependent perturbations with a lower gain. The mechanism of their amplification is also different from that of the 3D ones, which results from the coupling between Orr-Sommerfeld and Squire modes. Squire modes are not present in 2D so transient growth results exclusively from the combination of Orr-Sommerfeld modes, which offers fewer possible combinations and therefore achieves a lower maximum gain. In spite of this, some significant transient growth (up to two orders of magnitude) occurs for $\mathrm{Re}/\mathrm{Re}_c$ below unity. $G_{\max}$ is even between 7 (for $\mathrm{Re}/\mathrm{Re}_c=10^{-2}$) and 2.5 (for $\mathrm{Re}/\mathrm{Re}_c=1$) times greater than for the 2D Poiseuille flow ($H=0$) studied in Ref. 32. It is therefore reasonable to think that those optimal perturbations destabilize the flow at Reynolds numbers significantly smaller than Re_c, and even at lower $\mathrm{Re}/\mathrm{Re}_c$

than in the case $H=0$. These optimal modes are even more likely to be present in supercritical flows as $G_{\max}$ continues to increase as $(\mathrm{Re}/\mathrm{Re}_c)^{2/3}$ even for $\mathrm{Re}/\mathrm{Re}_c>1$, yielding gains of the order of 10^3.

The wavenumber of maximum transient growth $k_{G\max}$, and related time $t_{G\max}$ as a function of $\mathrm{Re}/\mathrm{Re}_c$ are reported in Fig. 12 for different values of H. As for the gain $G_{\max}$, the curves are quite close to each other and approach an asymptotic curve for high H. The time at which the optimal mode reaches maximal amplification $t_{G\max}$ quickly approaches a power law of the form $t_{G\max}H^{1/2}\sim(\mathrm{Re}/\mathrm{Re}_c)^{1/3}$ as $\mathrm{Re}/\mathrm{Re}_c$ increases for all values of H except $H=0$ for which $t_{G\max}\sim(\mathrm{Re}/\mathrm{Re}_c)^{1/3}$. When H tends to infinity, all curves merge into the same asymptotic one.

VI. CONCLUSION

We have investigated the quasi-2D stability of an MHD flow in a rectangular duct using the 2D model equation derived in Ref. 2 for flows in a transverse magnetic field. The terminology "quasi-2D" indicates here that although the whole study has been conducted using only two space variables, the three-dimensionality due to the presence of Hartmann layers is taken into account in the model through a linear friction term. This model equation provides a simple 2D model for the transition to turbulence in a duct, the dynamics of which can be studied over a wide range of parameters at little computational expense. The price to pay for this simplicity is that all perturbations are assumed to have a Hartmann profile along the direction of the magnetic field. The weak three-dimensionality in the base profile as well as 3D perturbations are therefore neglected so the focus is on the quasi-2D dynamics of those layers.

The critical modes for the linear stability analysis have been found to be antisymmetric Tollmien-Schlichting waves. In the limit $H\to\infty$ (in practice $H\gtrsim 200$), their linear stability is governed by the Reynolds number scaled on the thickness of the Shercliff layer $\mathrm{Re}/H^{1/2}$ with a critical value of 48350 providing a sufficient condition for stability (2D and 3D), and corresponding critical wavenumber $k_c/H^{1/2}=0.161532$. For $H\gtrsim 42$, a second type of unstable mode appears, made of three rows of vortices, symmetric about the duct axis. These parameters also govern the energy stability, which provides a sufficient condition for 2D stability, with critical parameters $\mathrm{Re}_E/H^{1/2}=65.3288$ and $k_E/H^{1/2}=0.86348422$. For values of Re between those two stability bounds, quasi-two-dimensional perturbations undergo some significant transient growth. Here again, an asymptotic regime is reached for H of a few hundred. For given H and Re, and in the limit $H\to\infty$, the maximum gain varies as $G_{\max}\sim(\mathrm{Re}/R_c)^{2/3}$, and it is achieved at time $t_{G\max}\sim H^{-1/2}(\mathrm{Re}/R_c)^{1/3}$ by perturbations of wavelength of the order of k_c. This transient growth mechanism results from combinations of Orr-Sommerfeld modes and differs from that happening in 3D Poiseuille flows where the more efficient interaction between Squire and Orr-Sommerfeld modes leads to a more significant transient growth, with $G_{\max}\sim\mathrm{Re}^2$. In the subcritical regime, however, $G_{\max}$ reaches values up to 100 and continues to increase in the supercritical regime. This indicates that quasi-2D perturbations most certainly destabilize the flow for values of Re much smaller than Re_c, but also that even in the supercritical regime, transient growth is more likely to drive the instability than normal mode exponential growth. The next step is then to perform some DNS of (1) in order to describe the nonlinear evolution of these optimal perturbations, and find out the critical value of Re at which they destabilize the base flow.

Now the next question is that of the implications of these results for the stability of the real 3D flow. This shall be our last point. The experiments of Ref. 1 have shown that the Hartmann layer in a duct such as that from Fig. 1 with $a/2L=1$ (so $H=\mathrm{Ha}/2$) becomes unstable for $\mathrm{Re}\geq\mathrm{Re}^{(H)}=380\mathrm{Ha}$. We have shown that in the same configuration, Shercliff layers are unstable to quasi-two-dimensional perturbations for $\mathrm{Re}\geq\mathrm{Re}^{(S)}=4.83\times10^4H^{1/2}$. For any $H>H_c=4047$, $\mathrm{Re}^{(S)}<\mathrm{Re}^{(H)}$. In other words, for $H>H_c$, the first instability to appear in the duct flow is that of the Shercliff layers, and not that of the Hartmann layers. The fact that quasi-2D perturbations undergo some significant transient growth in Shercliff layers for Re much lower than $\mathrm{Re}^{(S)}$ makes it likely that Shercliff layers become unstable to these perturbations at much lower Reynolds numbers. This, in turn, implies that the values H_c of H at which $\mathrm{Re}^{(S)}<\mathrm{Re}^{(H)}$ is much lower than 4047.

The author does not, however, believe this casts any doubt on the results obtained in Ref. 1, which have been closely recovered by the numerical simulations of Ref. 15. It is quite possible that the transition they identify is not one between a laminar duct flow and a flow with turbulent Hartmann layers but rather one between a quasi-2D turbulent flow with a stable Hartmann layer and a flow with turbulent Hartmann layers. Nevertheless, since the transition was detected by measuring the friction, one can be most assured that it is indeed a transition to turbulence in the Hartmann layer. The reason for this is that 2D turbulence involves mostly big vortices inducing a total friction that is hardly higher than that of the laminar state, and therefore very difficult to detect in their experiment. On the contrary, once turbulent, the Hartmann layer introduces strong three-dimensional perturbations responsible for a much higher friction.

This reasoning is of course only valid if the two-dimensional perturbations analyzed in this work are effectively responsible for the destabilization of the real 3D duct flow. Whether 3D perturbations not taken into account here play the leading role or whether the three-dimensionality of the base profile affects the growth of quasi-2D perturbations are to this day open questions and shall be answered by full 3D numerical simulations. In this regard, some recent work suggests that perturbations that are invariant along the magnetic field lines, similar to the optimal perturbations we find in this work, may well be the ones driving the instability as soon as Ha exceeds about 100. This question should now be investigated in the duct configuration.

[1] P. Moresco and T. Alboussière, "Experimental study of the instability of the Hartmann layer," J. Fluid Mech. **504**, 167 (2004).
[2] J. Sommeria and R. Moreau, "Why, how and when MHD turbulence be-

comes two-dimensional," J. Fluid Mech. **118**, 507 (1982).
[3]J. A. Shercliff, "Steady motion in conducting pipes under transverse magnetic fields," Proc. Cambridge Philos. Soc. **49**, 136 (1953).
[4]J. C. R. Hunt and K. Stewartson, "Magnetohydrodynamic flow in rectangular ducts II," J. Fluid Mech. **23**, 563 (1965).
[5]J. Hartmann, "Theory of the laminar flow in an electrically conductive liquid in a homogeneous magnetic field," Mat. Fys. Medd. K. Dan. Vidensk. Selsk. **15**, 34 (1937).
[6]J. A. Shercliff, "A simple demonstration of the Hartmann layer," J. Fluid Mech. **22**, 701 (1965).
[7]P. A. Davidson, "The role of angular momentum in the magnetic damping of turbulence," J. Fluid Mech. **336**, 123 (1997).
[8]R. C. Lock, "The stability of the flow of an electrically conducting fluid between parallel planes under a transverse magnetic field," Proc. R. Soc. London, Ser. A **233**, 105 (1955).
[9]M. Takashima, "The stability of the modified plane Poiseuille flow in the presence of a transverse magnetic field," Fluid Dyn. Res. **17**, 293 (1996).
[10]R. J. Lingwood and T. Alboussière, "On the stability of the Hartmann layer," Phys. Fluids **11**, 2058 (1999).
[11]K. B. Pavlov and S. L. Simkovich, "Stability of Hartmann flow with respect to two-dimensional perturbations of finite amplitude," Magnetohydrodynamics (N.Y.) **8**, 58 (1972).
[12]S. L. Simkhovich, "Influence of three-dimensional finite perturbations on the stability of Hartmann flow," Magnetohydrodynamics (N.Y.) **10**, 17 (1974).
[13]C. Airiau and M. Castets, "On the amplification of small disturbances in a channel flow with a normal magnetic field," Phys. Fluids **16**, 2991 (2004).
[14]D. Gerard-Varet, "Amplification of small perturbations in a Hartmann layer," Phys. Fluids **14**, 1458 (2002).
[15]D. Krasnov, E. Zienicke, O. Zikanov, T. Boeck, and A. Thess, "Numerical study of the instability of the Hartmann layer," J. Fluid Mech. **504**, 183 (2004).
[16]G. G. Branover, "Resistance of magnetohydrodynamics channels," Magnetohydrodynamics (N.Y.) **3**, 3 (1967).
[17]P. S. Lykoudis, "Transition between laminar and turbulent flow in magneto-fluid mechanics channels," Rev. Mod. Phys. **32**, 796 (1960).
[18]W. Murgatroyd, "Experiments on magneto-hydrodynamic channel flow," Philos. Mag. **44**, 1348 (1953).
[19]A. Pothérat, J. Sommeria, and R. Moreau, "An effective two-dimensional model for MHD flows with transverse magnetic field," J. Fluid Mech. **424**, 75 (2000).
[20]A. Pothérat, J. Sommeria, and R. Moreau, "Numerical simulations of an effective two-dimensional model for flows with a transverse magnetic field," J. Fluid Mech. **534**, 115 (2005).
[21]L. Bühler, "Instabilities in quasi two-dimensional magnetohydrodynamic flows," J. Fluid Mech. **326**, 125 (1996).
[22]M. Frank, L. Barleon, and U. Müller, "Visual analysis of two-dimensional magnetohydrodynamics," Phys. Fluids **13**, 2287 (2001).
[23]C. B. Reed and B. F. Picologlou, "Side wall flow instabilities in liquid metal MHD flow under blanket relevant conditions," Fusion Technol. **15**, 705 (1989).
[24]Y. Delannoy, B. Pascal, T. Alboussière, V. Uspenski, and R. Moreau, "Quasi-two-dimensional turbulence in MHD shear flows: The Matur experiment and simulations," in *Transfer Phenomena in Magnetohydrodynamic and Electroconducting Flows*, edited by A. Alemany, Ph. Marty, and J. P. Thibault (Kluwer Academic, Dordrecht, 1999).
[25]A. Thess, "Instabilities in two-dimensional periodic flows. Part III: Inviscid triangular lattice," Phys. Fluids A **5**, 335 (1993).
[26]P. J. Schmid and D. S. Henningson, *Stability and Transition in Shear Flows* (Spinger-Verlag, New York, 2001).
[27]L. M. Mack, "A numerical study of the temporal eigenvalue spectrum of the Blasius boundary layer," J. Fluid Mech. **73**, 497 (1976).
[28]J. J. Dongarra, B. Straughan, and D. W. Walker, "Chebyshev tau-qz algorithm methods for calculating spectra of hydrodynamic stability problems," Appl. Numer. Math. **22**, 399 (1996).
[29]P. A. Libby, A. Lundbach, and R. P. Harrington, "An experimental investigation of the isothermal laminar boundary layer on a porous flat plate," J. Appl. Spectrosc. **19**, 127 (1952).
[30]D. Joseph, *Stability of Fluid Motions* (Springer-Verlag, Berlin, 1976).
[31]F. H. Busse, "A property of the energetic stability limit for plane shear flow," Arch. Ration. Mech. Anal. **47**, 125 (1972).
[32]S. C. Reddy, P. J. Schmid, and D. S. Henningson, "Pseudospectra of the Orr-Sommerfeld operator," SIAM J. Appl. Math. **53**, 15 (1993).